

Supporting Information

Oriented Design of Triple Atom Catalysts for Electrocatalytic Nitrogen Reduction with the Genetic-algorithm-based Global Optimization Method Driven by First Principles Calculations

Wen Jing Li,^a Zhen Xin Lou,^a Hai Yang Yuan,^{*ab} Hua Gui Yang,^a Hai Feng Wang^{*b}

^aKey Laboratory for Ultrafine Materials of Ministry of Education, Shanghai Engineering Research Center of Hierarchical Nanomaterials, School of Materials Science and Engineering, East China University of Science and Technology, Shanghai 200237, China.

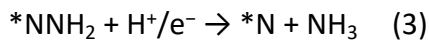
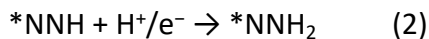
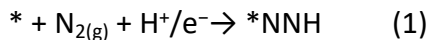
^bKey Laboratory for Advanced Materials, Research Institute of Industrial Catalysis and Centre for Computational Chemistry, School of Chemistry and Molecular Engineering, East China University of Science and Technology, Shanghai, 200237, China.

*E-mails: hfwang@ecust.edu.cn; hyyuan@ecust.edu.cn

Note S1 Calculation Method of Gibbs Free Energies of elementary steps in NRR

The adsorption energy (E_{ads}) can be calculated using the following equation: $\Delta E_{\text{ads}} = E_{\text{ads/sub}} - E_{\text{ads}} - E_{\text{sub}}$, where $E_{\text{ads/sub}}$, E_{ads} and E_{sub} are the total energies for the surface with species adsorbed, the adsorbed species and the clean surface, respectively. Here, ΔE_{ads} of the intermediates in NRR (e.g. NNH and NH₂) were represented by the energy of gaseous molecules of H₂ and NH₃. The adsorption free energy of the intermediates ($\Delta G(j)$) is calculated as: $\Delta G_{\text{ads}} = \Delta E_{\text{ads}} + \Delta E_{\text{ZPE}} - T\Delta S$, where ΔE_{ZPE} and $T\Delta S$ are the energy differences of the zero point energy and entropic contributions (see the detailed data in Table S2), which result from the vibrational frequencies; for the gaseous molecules (N₂, NH₃ and H₂), the entropy contributions of gaseous molecules ($T\Delta S$) are obtained with the experimental values¹.

The adsorption energies of 14 intermediates (*NNH, *NNH₂, *N, *NH, *NH₂, *NHNH, *NHNH₂, *NH₂NH₂, *N+*NH, *N+*NH₂, *NH+*NH, *NH+*NH₂, *NH₂+*NH₂ and *H, see Figure 1c) in NRR were calculated, which can be plotted as a function of the cohesive energy (E_c). Accordingly, the Gibbs free energy change ΔG_i of each elementary step can be written by $\Delta G_{\text{ads}}(j)$. For instance, the six elementary steps in the distal pathway of NRR were shown as follows:



The Gibbs free energy change ΔG_i of each step above can be written as:

$$\begin{aligned} \Delta G_1 &= E_{*NNH} - (E_{N_2} + E_{\text{slab}} + 0.5*E_{H_2}) + (\Delta ZPE - T\Delta S) \\ &= \Delta G(*NNH) + \Delta G_0 \end{aligned}$$

$$\begin{aligned} \Delta G_2 &= E_{*NNH_2} - (E_{*NNH} + 0.5*E_{H_2}) + (\Delta ZPE - T\Delta S) \\ &= \Delta G(*NNH_2) - \Delta G(*NNH) \end{aligned}$$

$$\begin{aligned} \Delta G_3 &= E_{*N} + E_{NH_3} - (E_{*NNH_2} + 0.5*E_{H_2}) + (\Delta ZPE - T\Delta S) \\ &= \Delta G(*N) - \Delta G(*NNH_2) \end{aligned}$$

$$\begin{aligned} \Delta G_4 &= E_{*NH} - (E_{*N} + 0.5*E_{H_2}) + (\Delta ZPE - T\Delta S) \\ &= \Delta G(*NH) - \Delta G(*N) \end{aligned}$$

$$\begin{aligned} \Delta G_5 &= E_{*NH_2} - (E_{*NH} + 0.5*E_{H_2}) + (\Delta ZPE - T\Delta S) \\ &= \Delta G(*NH_2) - \Delta G(*NH) \end{aligned}$$

$$\Delta G_6 = E_{\text{slab}} + E_{NH_3} - (E_{*NH_2} + 0.5*E_{H_2}) + (\Delta ZPE - T\Delta S)$$

$$= -\Delta G(*\text{NH}_2)$$

where $\Delta G(*\text{NNH})$, $\Delta G(*\text{NNH}_2)$, $\Delta G(*\text{N})$, $\Delta G(*\text{NH})$ and $\Delta G(*\text{NH}_2)$ are the Gibbs adsorption energies of $*\text{NNH}$, $*\text{NNH}_2$, $*\text{N}$, $*\text{NH}$ and $*\text{NH}_2$ on active centers and calculated related to NH_3 and H_2 . Here, the computational hydrogen electrode model was used to present the chemical potential of a proton-electron pair (H^+/e^-) at any given pH and applied potential U (vs. the reversible hydrogen electrode).² In this approach, the chemical potentials of a proton-electron pair (H^+/e^-) and a H_2 molecule are equilibrated at 0 V (vs. RHE) at all pH values.¹⁻² ΔG_0 is the Gibbs free change of reaction ($\text{N}_2 + 3\text{H}_2 \rightarrow 2\text{NH}_3$). The effect of the potential on the state with an electron involved was considered by shifting the energy of $-eU$.

Note S2 Designing Method of TAS

Here we used the developed CATIDPy software which is genetic-algorithm-based (GA) global optimization method³ to seek the feasible composition of TAS according to the activity descriptor $\Delta G(*N)$, where the whole process involves some evolutionary principles, such as selection, crossover and mutation, and a relatively small modification or transformation of the structure. Here, we compiled the GA process according to the genetic principle, and customized the doping operator. A wide variety of potential catalytic materials were subsequently generated via evolutionary operators, in which the on-the-fly DFT calculations can be automatically performed to investigate the potential activity of TAS catalyst for NRR based on GA. The fitness function in our calculated process is defined as $1/|\Delta G(*N) - \Delta G_{\text{opt}}(*N)|$, where $\Delta G(*N)$ is the adsorption energy of N atom on different TAS, and $\Delta G_{\text{opt}}(*N)$ is the optimal adsorption energy N atom on TAS with the optimal catalytic activity.

Specifically, there are mainly four of the whole automated and object-oriented workflows in CATIDPy to screen TAS catalysts for NRR, which can be described as follows:

- (i) The basal surface unit cell can be obtained from designed programs;
- (ii) the center of a hollow site is substituted by metals from the database according to the structural-gene-represented string, generated by GA, and then relaxed the surface unit cells;
- (iii) the adsorption structure of N atom is optimized on the designed configuration, and the DFT results are stored in a database for calculating $\Delta G(*N)$;
- (iv) the metal atoms are automatically selected and updated following the direction determined by GA, and this yields a closed feedback loop of high-throughput screening.

Note S3 The effect of magnetism.

In order to further verify the magnetism effects in our reaction system, we explored the total energy change of key intermediates in NRR following the distal pathway on Co double/Triple-atom structures specified with ferromagnetism (FM) or antiferromagnetism (AFM) on Co atoms as examples compared with the one from the built-in spin-polarization method in VASP code. Here, we allowed the spin-state to be fully optimized during the structural optimizations by invoking the built-in spin-polarization parameter in VASP code; such a strategy has been used widely in atom-dispersed catalysts. As shown in Table S3 and Table S4, we can find that all the intermediate states from the automatic optimization method for magnetism in VASP give the similar energies and magnetic orders with ferromagnetism (FM) set in Co double/Triple-atom systems, which have the most stable energies. Generally, the built-in spin-polarization method for magnetism in VASP can basically generate the most stable state of each structure; the small changes of obtained energies from DFT calculations do not affect the identifications of the whole catalytic trends.

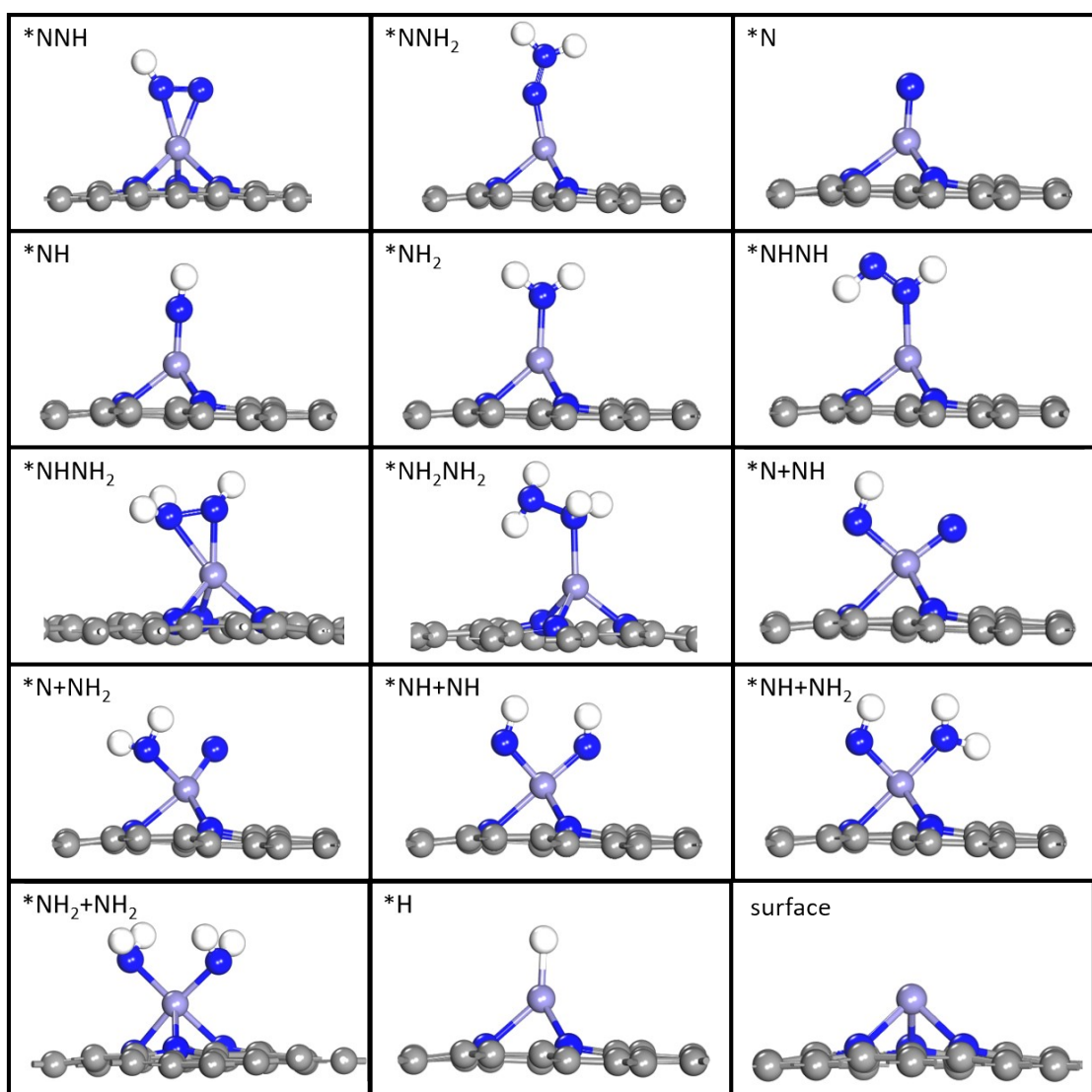


Figure S1. Intermediates in NRR on SAS.

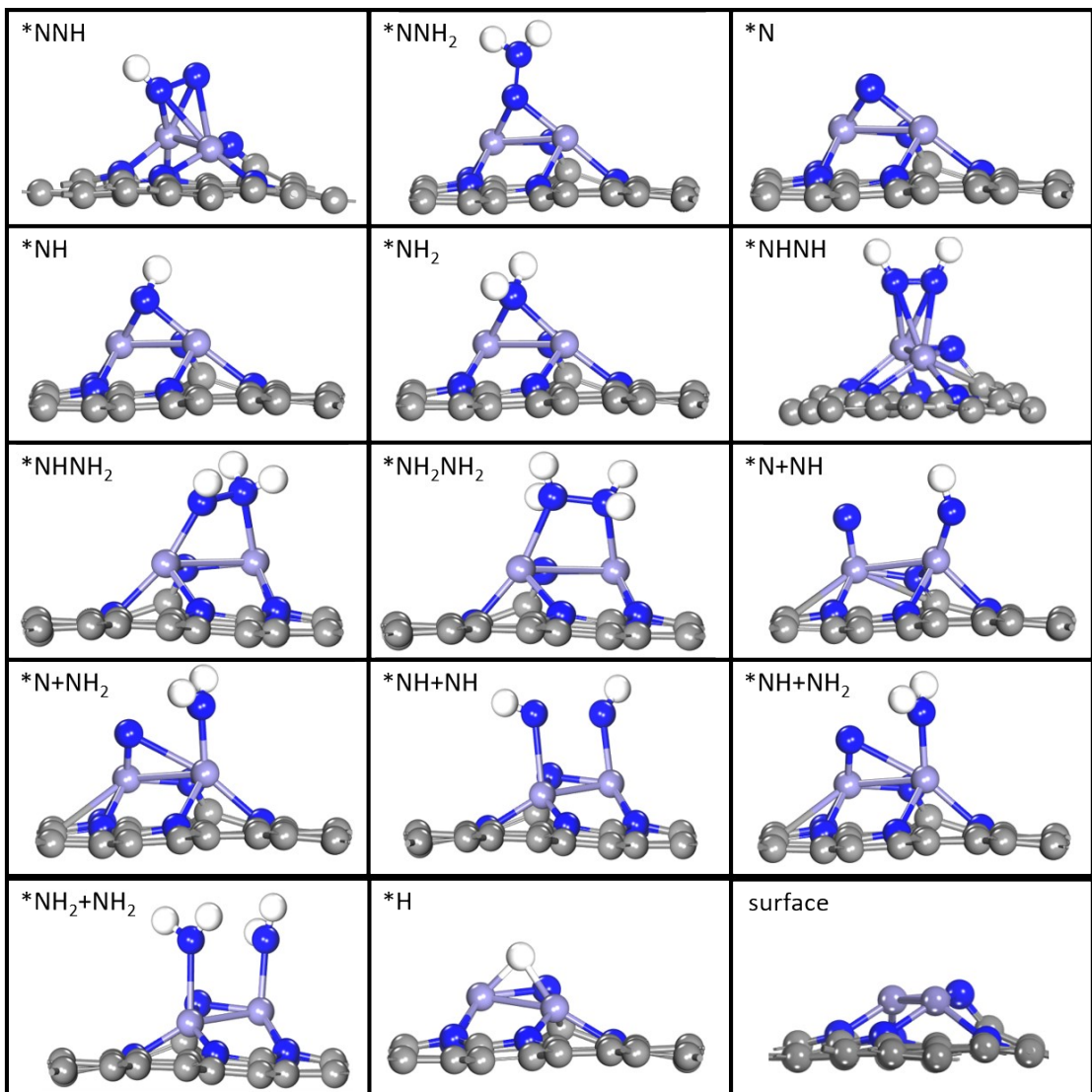


Figure S2. Intermediates in NRR on DAS.

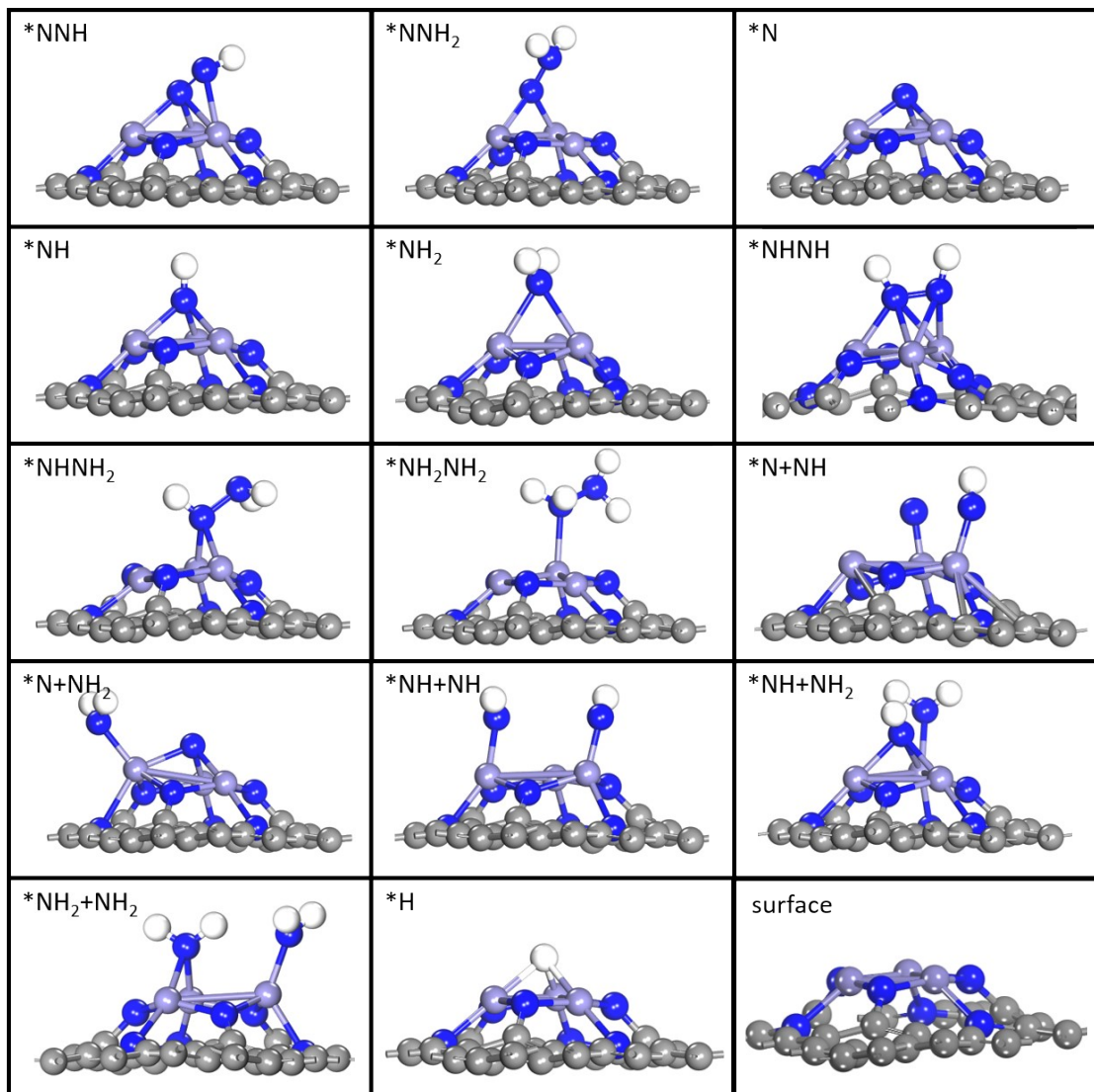


Figure S3. Intermediates in NRR on TAS.

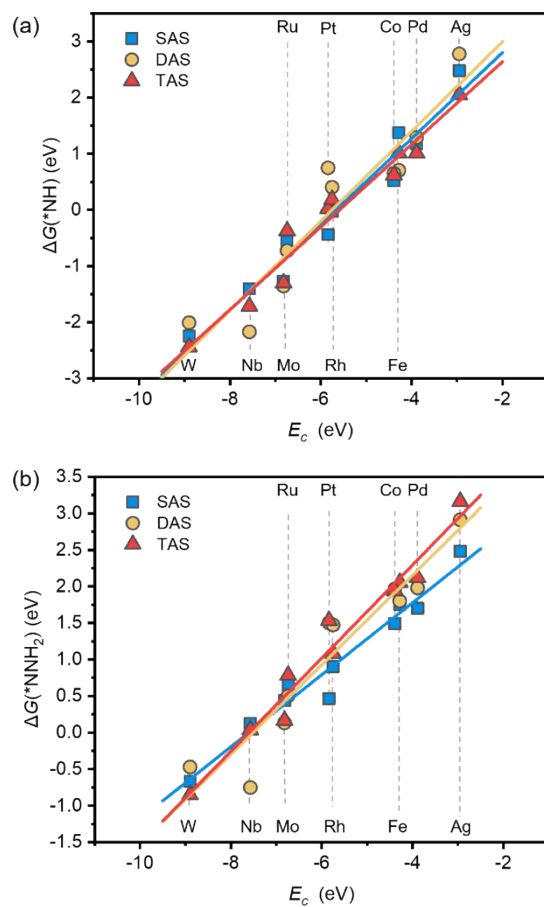


Figure S4. Relationships for the adsorption energies of intermediates ${}^*\text{NH}$ (a) and ${}^*\text{NNH}_2$ (b) as a function of E_c .

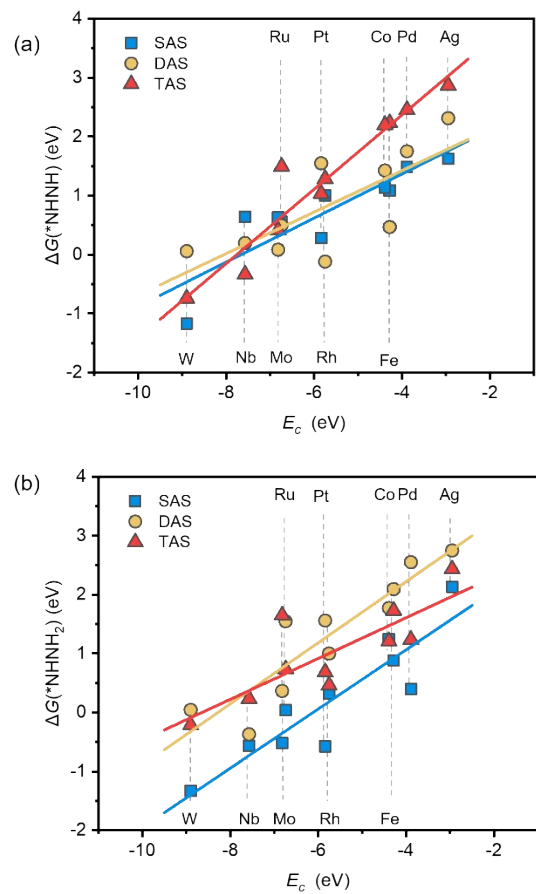


Figure S5. Relationships for the adsorption energies of intermediates ${}^*\text{NHNH}$ (a) and ${}^*\text{NHNH}_2$ (b) as a function of E_c .

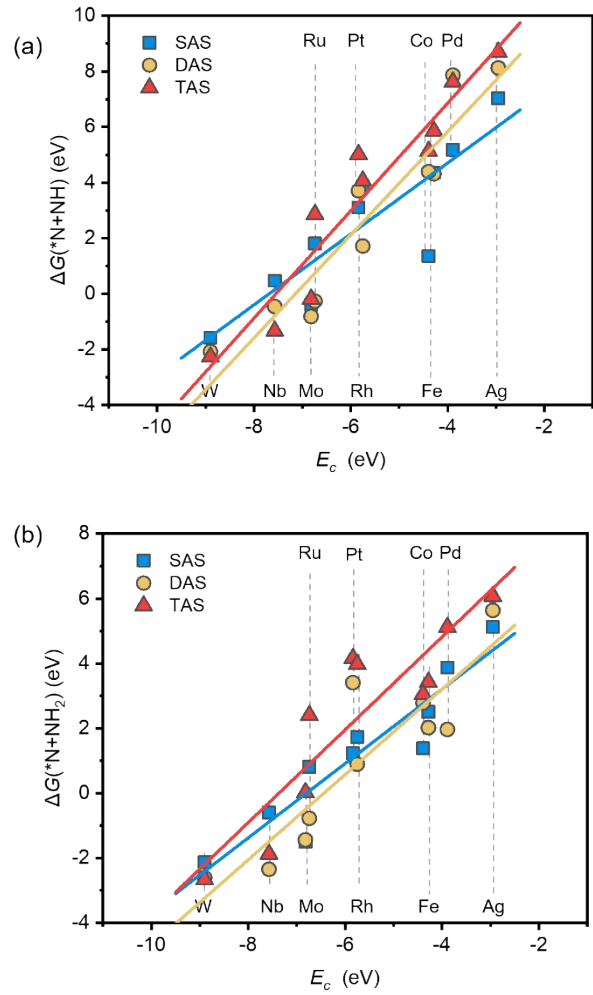


Figure S6. Relationships for the adsorption energies of intermediates $*\text{N}+\text{NH}$ (a) and $*\text{N}+\text{NH}_2$ (b) as a function of E_c .

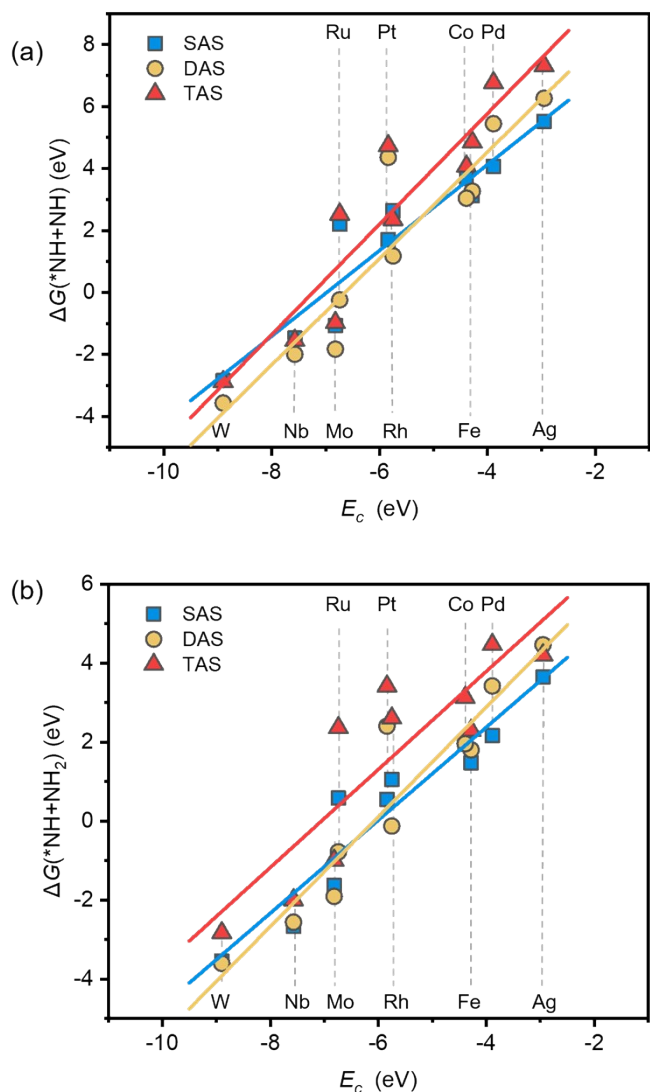


Figure S7. Relationships for the adsorption energies of intermediates ${}^*\text{NH}+\text{NH}$ (a) and ${}^*\text{NH}+\text{NH}_2$ (b) as a function of E_c .

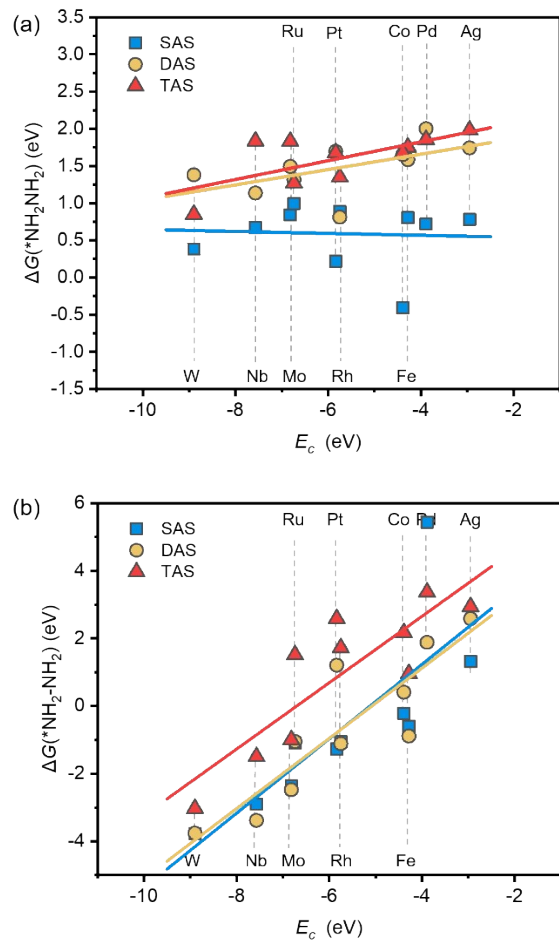


Figure S8. Relationships for the adsorption energies of intermediates $*\text{NH}_2\text{NH}_2$ (a) and $*\text{NH}_2\text{-NH}_2$ (b) as a function of E_c .

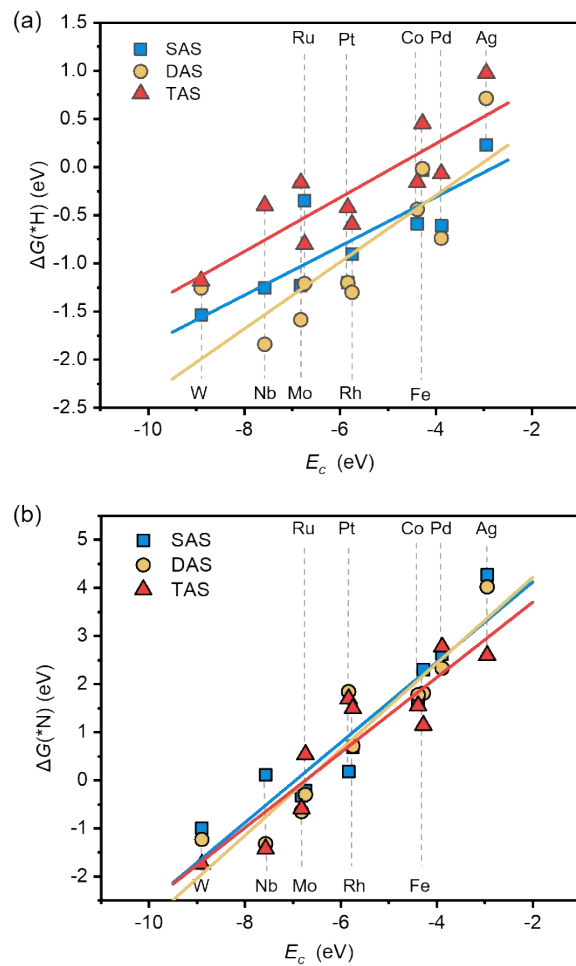


Figure S9. Relationships for the adsorption energies of intermediates $*\text{H}$ (a) and $*\text{N}$ (b) as a function of E_c .

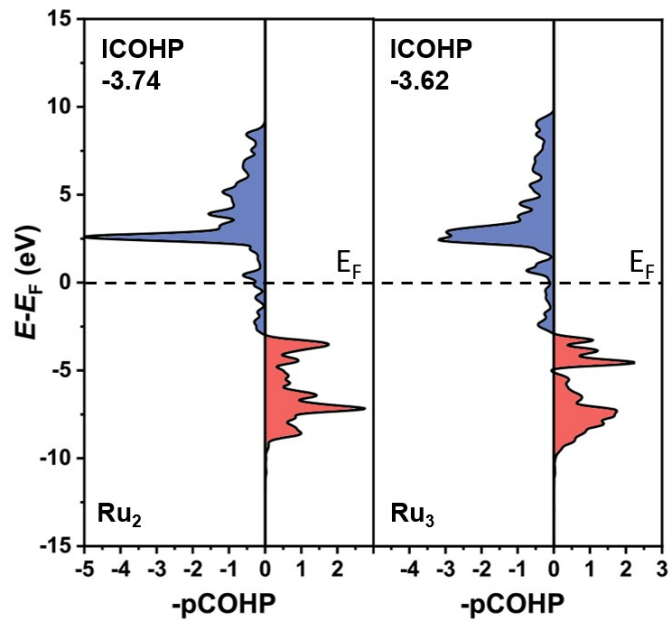


Figure S10. Projected crystal orbital Hamilton population (pCOHP) between Ru atom and N atom in $*\text{NH}_2$ adsorbed on Ru_2 and Ru_3 , with negative (bonding) contributions at the right part and positive (antibonding) contributions at the left part, respectively.

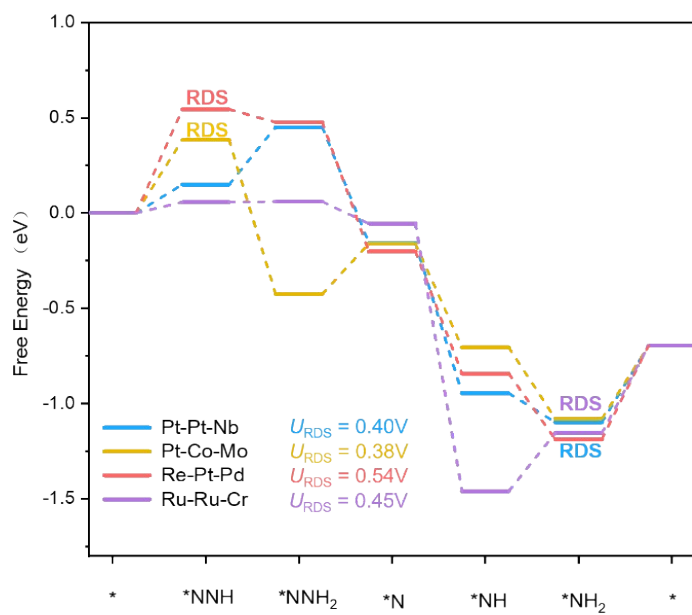


Figure S11. Energy profiles of NRR on Pt-Pt-Nb, Pt-Co-Mo, Re-Pt-Pd and Ru-Ru-Cr TAS at a potential of 0 V (vs. RHE) and pH = 0.

Table S1. The specific applied U - J value (U_{eff}) of 3d metals for DFT calculations.⁴

3d	Sc	Ti	V	Cr	Mn	Fe	Co	Ni	Cu	Zn
U_{eff}	2.11	2.58	2.72	2.79	3.06	3.29	3.42	3.40	3.87	4.12

Table S2. Zero-point energies (*ZPE*) and entropy (*TS*) of different adsorption species and gas molecules at 298.15 K.

	SAS		DAS		TAS	
	<i>ZPE</i>	<i>TS</i>	<i>ZPE</i>	<i>TS</i>	<i>ZPE</i>	<i>TS</i>
*NNH	0.97	0.29	1.30	0.32	0.61	0.30
*NNH ₂	1.24	0.25	1.64	0.40	0.96	0.39
*N	0.57	0.16	0.91	0.27	0.21	0.27
*NH	0.68	0.23	1.20	0.28	0.54	0.25
*NH ₂	1.12	0.25	1.48	0.33	0.87	0.27
*NNHH	0.81	0.17	1.57	0.40	0.96	0.28
*NNHH ₂	1.21	0.23	2.23	0.43	1.34	0.30
*NH ₂ NH ₂	1.49	0.21	2.23	0.43	1.65	0.44
*N+*NH	0.87	0.19	1.21	0.36	1.23	0.49
*N+*NH ₂	1.17	0.23	1.54	0.45	1.71	0.53
*NH+*NH	1.11	0.22	1.45	0.43	1.65	0.53
*NH+*NH ₂	1.42	0.26	1.80	0.46	1.99	0.47
*NH ₂ +*NH ₂	1.71	0.32	2.07	0.54	2.44	0.54
Surface	0.46	0.15	0.78	0.40	0.13	0.23
H ₂	0.27	0.41	\	\	\	\
N ₂	0.15	0.59	\	\	\	\
NH ₃	0.91	0.60	\	\	\	\

Table S3. The total energy (in eV) and magnetic moments (in μ_B) for each atom (δ_1, δ_2) of each key intermediate in NRR following the distal pathway on Co double atom structures (DAS) with ferromagnetism (FM) or antiferromagnetism (AFM). AM represents that the magnetism of the structure is optimized by the built-in spin-polarization method in VASP code.

	AM			FM			AFM		
	Energy	δ_1	δ_2	Energy	δ_1	δ_2	Energy	δ_1	δ_2
*NNH	-301.44	0.83	1.08	-301.44	0.83	1.08	-301.43	1.03	-0.90
*NNH ₂	-304.80	1.36	1.39	-304.80	1.36	1.39	-304.71	1.70	-0.90
*N	-288.59	1.18	1.18	-288.59	1.18	1.18	-288.44	1.12	-1.13
*NH	-293.45	1.32	1.32	-293.45	1.32	1.32	-293.30	1.48	-0.68
*NH ₂	-298.38	0.97	0.97	-298.39	0.98	0.98	-298.38	0.95	-0.95
surface	-281.33	1.16	1.66	-281.33	1.16	1.66	-281.32	-1.36	0.26

Table S4. The total energy (in eV) and magnetic moments (in μ_B) for each atom (δ_1 , δ_2 and δ_3) of each key intermediate in NRR following the distal pathway on Co triple atom structures (TAS) with ferromagnetism (FM) or antiferromagnetism (AFM). AM represents that the magnetism of the structure is optimized by the built-in spin-polarization method in VASP code.

	AM				FM				AFM			
	Energy	δ_1	δ_2	δ_3	Energy	δ_1	δ_2	δ_3	Energy	δ_1	δ_2	δ_3
*NNH	-295.27	1.29	1.19	-0.93	-295.27	1.29	1.19	-0.94	-295.27	1.29	1.19	-0.93
*NNH ₂	-298.78	-0.81	1.08	0.51	-298.78	-0.81	1.07	0.51	-298.78	-0.79	1.08	0.51
*N	-282.75	1.54	1.54	1.54	-282.75	1.54	1.53	1.54	-282.64	1.48	1.48	-1.36
*NH	-287.48	1.29	1.29	1.29	-287.48	1.29	1.28	1.29	-287.48	1.29	1.29	1.29
*NH ₂	-291.89	0.95	1.04	1.04	-291.89	0.95	1.04	1.03	-291.88	1.25	-0.22	-1.05
surface	-275.37	1.33	1.40	1.41	-275.37	1.32	1.41	1.41	-275.31	1.60	1.59	-0.78

Table S5. Bonding length between ligand N and active metal center on single, double and triple atomic catalysts, the unit is Å.

	Fe	Co	Nb	Mo	Ru	Rh	Ag	W	Pd	Pt
SAS	2.01	1.84	2.02	1.97	1.92	2.05	2.29	2.03	2.11	2.10
DAS	1.96	1.87	2.00	2.06	2.05	1.99	2.38	2.09	2.14	2.14
TAS	1.82	1.76	1.98	1.95	1.91	1.93	2.03	1.96	1.93	1.94

Table S6. The corresponding cohesive energies (E_c) from experimental ($E_c^{\text{exp.}}$) values.⁵

Metal	$E_c^{\text{exp.}}$
Ti	-4.85
Zr	-6.25
Hf	-6.44
V	-5.31
Nb	-7.57
Ta	-8.10
Cr	-4.10
Mo	-6.82
W	-8.90
Mn	-2.92
Re	-8.03
Fe	-4.28
Ru	-6.74
Os	-8.17
Co	-4.39
Rh	-5.75
Ir	-6.94
Ni	-4.44
Pd	-3.89
Pt	-5.84
Cu	-3.49
Au	-3.81
Ag	-2.95

Table S7. List of 163 TAS for NRR. E_f and U_{dis} are formation energy and dissolution potential, respectively.

TAS	$\Delta G(\text{*N})$	E_f	U_{dis}	TAS	$\Delta G(\text{*N})$	E_f	U_{dis}
RhOsTa	0.15	-1.43	0.80	RhAuRe	0.49	-0.61	0.65
IrMoRe	0.15	-1.10	0.79	ReAuRh	0.49	-0.61	0.65
ReMolr	0.15	-1.10	0.79	VWAu	0.51	-0.39	0.15
TaRuRu	0.17	-1.45	0.63	HfAuRu	0.51	-1.76	0.14
RuTaRu	0.17	-1.45	0.63	PtMoPt	0.52	-1.37	1.18
RuMnTi	0.17	-1.36	-0.10	AuTaPt	0.53	-1.40	0.75
CoWPt	0.18	-1.07	0.76	RhNiTc	0.53	-0.79	0.64
WCoPt	0.18	-1.07	0.76	FeCrCr	0.54	-0.20	-0.65
IrMnTc	0.19	-0.82	0.62	RuMoCo	0.55	-1.17	0.47
IrMnTc	0.19	-0.82	0.62	MoPdPt	0.56	-1.42	1.13
HfCuRu	0.19	-1.67	0.05	ReAuCr	0.57	-0.26	0.14
AuTaV	0.19	-0.84	0.05	ZrAuCr	0.57	-1.62	-0.17
OsCoV	0.19	-0.35	0.47	CuMoRh	0.58	-1.03	0.63
PdNiW	0.21	-0.98	0.65	RhMoCu	0.58	-1.04	0.63
MnPtRe	0.22	-0.69	0.42	RhPdRe	0.58	-1.06	1.03
RuTaCu	0.23	-1.27	0.52	RhCoTc	0.58	-0.95	0.71
RuMoNi	0.24	-1.05	0.42	RhCoTc	0.58	-0.95	0.71
HfCoFe	0.24	-1.41	-0.43	RhRePd	0.58	-1.06	1.03
MoCuOs	0.25	-0.79	0.71	RePdRh	0.58	-1.06	1.03
TcRuRe	0.25	-0.98	0.80	RePdRh	0.58	-1.06	1.03
RhRuTi	0.25	-1.47	0.54	RePdRh	0.58	-1.06	1.03
PdWPt	0.26	-1.29	1.21	RhTaRh	0.58	-1.77	0.85
OsNbIr	0.26	-1.32	0.78	OsWIr	0.59	-0.94	0.95
ReAuIr	0.26	-0.40	0.76	WAuPt	0.59	-0.79	0.79
TaFePt	0.26	-1.27	0.49	PtMoNi	0.60	-1.13	0.66
IrAuRe	0.26	-0.40	0.76	PtMoAg	0.60	-1.08	0.97
FeNbIr	0.26	-1.16	0.34	MoAgPt	0.61	-1.08	0.97
FeWPt	0.27	-0.77	0.58	RhPtRe	0.61	-1.01	1.07
MoNiOs	0.27	-0.89	0.63	NbCoPt	0.65	-1.64	0.49
TcCoRe	0.27	-0.98	0.58	ReAuRe	0.65	-0.43	0.48
ZrCoFe	0.28	-1.38	-0.39	OsAuRe	0.65	-0.41	0.72
RhNbFe	0.28	-1.27	0.11	ReAuOs	0.65	-0.41	0.72
RuZrCo	0.28	-1.82	0.00	PdHfOs	0.66	-1.84	0.57
CrCrFe	0.29	-0.14	-0.68	WPtRe	0.66	-1.05	0.84
IrCrTc	0.30	-0.77	0.68	HfAuCr	0.66	-1.68	-0.19
PdCoRe	0.30	-0.81	0.67	HfAuCr	0.66	-1.68	-0.19
RhNbRu	0.31	-1.60	0.52	FeTiNi	0.68	-0.93	-0.32
TcAuRu	0.31	-0.56	0.66	AuTaPd	0.68	-1.47	0.72
PdCoW	0.32	-1.14	0.72	ReTcOs	0.69	-0.83	0.84
RuNbAg	0.32	-1.37	0.42	RhCoMo	0.69	-1.32	0.57
MoCoCu	0.33	-0.83	0.29	RhTiRh	0.70	-1.59	0.65
RuNbFe	0.34	-1.15	0.02	RhRhW	0.70	-1.38	0.98
TcReRe	0.35	-0.88	0.66	NiNbPt	0.71	-1.54	0.45
RuTaRh	0.36	-1.62	0.74	MoRePt	0.72	-1.18	0.78
RhRuTa	0.36	-1.62	0.74	MoPtRe	0.72	-1.18	0.78
IrMoTc	0.36	-1.32	0.95	RhAuMo	0.72	-1.08	0.64
CrTaCu	0.37	-0.96	-0.01	WTcPt	0.73	-1.29	1.05

CoReRe	0.37	-0.80	0.45	WOsNi	0.73	-0.78	0.68
NbAuCr	0.39	-1.11	-0.07	CoCoHf	0.74	-1.82	-0.23
RuNbCo	0.39	-1.47	0.21	NbAuPt	0.74	-1.42	0.57
MoCoOs	0.39	-1.02	0.66	RuAuRe	0.75	-0.61	0.61
RuCrRh	0.39	-0.61	0.35	RuCoCr	0.75	-0.56	0.04
RhOsW	0.39	-1.06	0.88	IrAgPd	0.75	-0.82	1.44
TiCoCo	0.39	-1.23	-0.12	PtAuHf	0.76	-1.93	0.35
ReReRe	0.41	-0.70	0.53	PtCrTc	0.76	-0.88	0.66
RhOsMo	0.41	-1.16	0.83	RhIrW	0.76	-1.29	1.10
PdHfCr	0.41	-1.99	-0.02	RhWIr	0.77	-1.29	1.10
VAuNb	0.41	-0.87	-0.12	RhWIr	0.77	-1.29	1.10
RhNiRe	0.42	-0.73	0.53	RhTcRe	0.77	-1.13	0.90
CoPtRe	0.42	-0.78	0.72	RhReTc	0.77	-1.13	0.90
RuMnRh	0.42	-0.79	0.35	CuNbIr	0.79	-1.29	0.59
PtCoRe	0.42	-0.78	0.72	IrNbPt	0.79	-1.69	0.95
NiPtRe	0.43	-0.66	0.67	NbIrPt	0.80	-1.69	0.95
RhCoRe	0.43	-0.87	0.59	RhZrRh	0.80	-2.11	0.37
RhReCo	0.43	-0.87	0.59	RhRhMo	0.80	-1.44	0.88
MoCoAg	0.43	-0.92	0.40	RhNbPt	0.80	-1.82	0.82
RhRuV	0.43	-0.61	0.40	HfAuMn	0.80	-1.74	-0.24
RhRuW	0.43	-1.23	0.87	RhWNi	0.81	-1.12	0.61
IrWAu	0.43	-0.80	0.83	RhNiW	0.81	-1.12	0.61
RhReRe	0.45	-0.95	0.73	MoTcPt	0.82	-1.40	0.97
RhOsNi	0.45	-0.49	0.74	AgMnHf	0.82	-1.72	-0.37
RhWAu	0.45	-0.94	0.70	RuTaPd	0.83	-1.68	0.86
NiNbCo	0.46	-1.26	-0.09	RuTaPd	0.83	-1.68	0.86
RuCrRu	0.47	-0.19	0.32	RhAuOs	0.83	-0.43	0.80
ReReRh	0.47	-0.95	0.73	OsAuRh	0.83	-0.43	0.80
PtNbPt	0.47	-1.05	0.96	RuCoRe	0.83	-0.91	0.57
PdRePt	0.47	-0.97	1.15	NiAuW	0.84	-0.55	0.33
MoCoPt	0.47	-1.23	0.70	ReRuOs	0.84	-0.81	0.84
RuMoRh	0.48	-1.31	0.78	OsRuRe	0.84	-0.81	0.84
RhNbIr	0.48	-1.65	0.79	RuReCo	0.84	-0.91	0.57
RhTalr	0.48	-1.66	0.98	RhVlr	0.84	-0.65	0.73
IrNbIr	0.49	-1.54	0.92				

Table S8. Performance comparisons between TAS catalysts in this work and previously reported representative electrocatalysts for NRR.

Catalyst and type	Limiting potential (vs. RHE)	Reference
Pt-Pt-Nb TAS	0.40	
Pt-Co-Mo TAS	0.38	This work
Pt-Pd-Re TAS	0.54	
Ru-Ru-Cr TAS	0.45	
Mo@BN SAS ⁶	0.35	<i>J. Am. Chem. Soc.</i> 2017 , <i>139</i> , 12480–12487
Mo ₁ @N ₃ -G SAS ⁷	0.50	<i>ACS Catal.</i> 2019 , <i>9</i> , 3419–3425
Ti@C ₂ N SAS ⁸	0.54	<i>EcoMat.</i> 2020, <i>2</i> , e12014
V ₂ -Pc ⁹	0.39	<i>J. Am. Chem. Soc.,</i> 2020 , <i>142</i> , 5709–5721.
Fe ₂ -N ₂ ¹⁰	0.39	<i>J. Phys. Chem. C</i> 2019 , <i>123</i> , 19066–19076
Ru(0001) ¹¹	1.40	<i>ACS Catal.</i> 2019 , <i>9</i> , 11137–11145
Au(110) ¹²	1.10	<i>J. Am. Chem. Soc.</i> 2019 , <i>141</i> , <i>45</i> , 18264–18270

Reference

1. M. W. Chase Jr, *NIST-JANAF Thermochemical Tables , Fourth Edition, J. Phys. Chem. Ref. Data, Monograph 9*, 1998, 1-1951.
2. J. K. Norskov, J. Rossmeisl, A. Logadottir, L. Lindqvist, J. R. Kitchin, T. Bligaard and H. Jonsson, *J. Phys. Chem. B*, 2004, **108**, 17886-17892.
3. C. Zhou, J. Y. Zhao, P. F. Liu, J. Chen, S. Dai, H. G. Yang, P. Hu and H. Wang, *Chem. Sci.*, 2021, **12**, 10634-10642.
4. C. Y. Lin, L. Zhang, Z. Zhao and Z. Xia, *Adv. Mater.*, 2017, **29**, 1606635.
5. X. Guo, J. Gu, S. Lin, S. Zhang, Z. Chen and S. Huang, *J. Am. Chem. Soc.*, 2020, **142**, 5709-5721.
6. J. Zhao and Z. Chen, *J. Am. Chem. Soc.*, 2017, **139**, 12480-12487.
7. W. Zhao, L. Zhang, Q. Luo, Z. Hu, W. Zhang, S. Smith and J. Yang, *ACS Catal.*, 2019, **9**, 3419-3425.
8. Y. Qian, Y. Liu, Y. Zhao, X. Zhang and G. Yu, *EcoMat*, 2020, **2**, e12024.
9. X. Guo, J. Gu, S. Lin, S. Zhang, Z. Chen and S. Huang, *J. Am. Chem. Soc.*, 2020, **142**, 5709–5721.
10. D. Ma, Z. Zeng, L. Liu, X. Huang and Y. Jia, *J. Phys. Chem. C*, 2019, **123**, 19066-19076.
11. E. Tayyebi, Y. Abghoui and E. Skúlason, *ACS Catal.*, 2019, **9**, 11137-11145.
12. C. Ling, Y. Zhang, Q. Li, X. Bai, L. Shi and J. Wang, *J Am Chem Soc*, 2019, DOI: 10.1021/jacs.9b09232.